13.5 Impact of Microphysical Parameterizations on Supercell Thunderstorm Cold Pools using WRF-DART Experiments

Anthony E. Reinhart*, Christopher C. Weiss,
Texas Tech University, Lubbock, Texas

David C. Dowell
NOAA/ESRL, Boulder, Colorado

1. Introduction

Microphysical parameterizations are essential to proper mesoscale and storm scale modeling. The limitations of current parameterizations are quickly being realized and updated with new findings. However, as with all parameterizations deficiencies are present.

Limitations in the microphysical parameterizations can contribute significant error to numerical simulations of storms. Even seemingly subtle differences between different yet sophisticated microphysical parameterizations effect radically different results (Morrison and Milbrandt 2011; Bryan and Morrison 2012). However, surface observations have not been used to directly verify these parameterizations, owing mainly to insufficient spatial and temporal resolution to provide a robust result.

Bulk microphysical parameterizations are currently used in most NWP models due to their computational efficiency and will be used in this study. Bulk microphysical parameterizations typically use a gamma or exponential function to represent the particle size distribution (PSD) for several categories of hydrometeor species. One or more free parameters of the represented function relates back to the mixing ratio in single-moment parameterizations and mixing ratio and number concentration in two-moment parameterizations. This study will examine two different two-moment microphysical parameterizations; the Morrison scheme and the Milbrandt-Yau (MY) scheme (Milbrandt and Yau 2005, 2006a,b; Morrison et al. 2009). There are many subtle differences between the two parameterizations and are highlighted by Morrison and Milbrandt (2011). One major difference between the two parameterizations is the addition of a separate hail species in the MY scheme compared to just a graupel species in the Morrison scheme.

The Verification of the Origins of Rotation in Tornadoes EXperiment 2 (VORTEX2) provides the opportunity to collect the data needed to verify how well the microphysical parameterizations are preforming

*Corresponding author address: Anthony E. Reinhart, Texas Tech University, Atmospheric Science Group, Department of Geosciences, Lubbock, TX, 79409; e-mail: anthony.reinhart@ttu.edu

thermodynamically at the surface, more specifically how accurately the supercell cold pool is being simulated. The cold pool of even the simplest air mass thunderstorm, let alone the complex thermodynamic and kinematic structure of a supercell thunderstorm, has great importance on many aspects of its parent storm (e.g. longevity, propagation, and evolution).

VORTEX2 intercepted a long-lived cyclic supercell in Northern Texas between 2230 UTC and 0130 UTC on 18 May 2010. Data from many VORTEX2 teams were collected on this supercell throughout the supercells' life cycle and several datasets are used in this study. The Shared Mobile Atmospheric Research and Teaching Radar (SMART-R) (Biggerstaff et al. 2005) collected data from 2230 UTC through 0100 UTC and are used to supplement the WSR-88D data from Amarillo, Texas, allowing for more structure of the supercell to be realized in the simulation.

StickNets are deployable in-situ instruments that collect thermodynamic and kinematic variables at 1 Hz. Twenty-four StickNets were deployed in two deployments (arrays) during 18 May 2010. This study will look at the period of the first array deployment between 2222 UTC and 2302 UTC with the supercell updraft passing over the array at approximately 2330 UTC. The StickNet array spans 30 km in the north-south direction with a 1.5 km spacing (except in the city of Dumas where there is a 6 km area where no probes could be deployed) allowing for a complete sample of the observed supercell cold pool and will be used as truth for the verification of the simulated supercell cold pool.

2. Methodology

The real data simulations are initialized using the one-half degree GFS forecast from 0000 UTC on 18 May 2010 and interpolated onto the 1 km domain. The Weather and Forecasting model version 3.3.1 (WRF) is used in this study (Skamarock et al. 2005). The two microphysical schemes used in this verification are the Morrison parameterization and the MY parameterization. The Yansei University (YSU) planetary boundary layer parameterization is used along with the Noah land surface model.

The Data Assimilation Research Testbed (DART) is a software program that allows for the use of an ensemble Kalman filter technique that can ingest observations and keep the model closer to truth by altering the covariances between the state variables. The ensemble size is 50 members and each member has random perturbations added to the boundary conditions and a noise was added in areas where the observed reflectivity was greater than 25 dBZ (Dowell and Wicker 2009) to maintain ensemble spread.

Data assimilated in this study are radial velocities from the WSR-88D and SMART-R, while clear-air reflectivity values were assimilated from the WSR-88D. Data are assimilated into the model every two minutes. Clear-air reflectivity values help to dampen and remove spurious convection that the model wants to produce. The radial velocities are cleaned to remove ground clutter, anomalous propagation, and other data artifacts. These data are then objectively analyzed onto a 2 km grid using a two pass Barnes scheme with a smoothing parameter of 2 and a convergence parameter of 0.3.

The simulations began at 2100 UTC on 18 May 2010 approximately one hour prior to initiation of the target supercell, allowing for ample time to develop the flow-dependent features of the ensemble and properly evolve mesoscale features. The simulation ran through 0000 UTC on 19 May 2010, which is after the supercell crosses the StickNet array.

StickNet data from the first deployment array were quality controlled and decimated to one-second resolution where necessary. To verify the model field, the StickNet data are converted to a grid using time-to-space conversion and then a two pass Barnes scheme is applied. The resulting field is a contour of the observed supercell cold pool over a 50-minute period from 2300 – 2350 UTC on 18 May 2010.

The verification of the simulated supercell cold pool happens in three areas: the forward flank, rear flank, and location of the maximum negative temperature within the cold pool. Here the forward flank is the area to the right of the updraft and mesocyclone and the rear flank is the area to the left of the updraft and mesocyclone (Fig. 1). The cold pool is defined as the area that is 1 degree cooler than the inflow environment. The forward flank and rear flank cold pools are verified separately as each develop through different processes. Separating the supercell cold pool into two regions allows for more in depth reasoning as to why a parameterization may be accurate or inaccurate. The two separate flanks of the supercell cold pool are then averaged and compared to the average StickNet values.

3. Results

Morrison Parameterization

The simulation for the Morrison microphysical parameterization produces a supercell close to the location of that observed at 2326 UTC (Fig. 2). The reflectivity of the supercell simulated is similar to the observed supercell from the SMART-R at verification time.

Verification of the maximum virtual potential temperature deficit reveals that the simulation has a warmer cold pool than observed by the StickNets. A maximum virtual potential temperature perturbation deficit of 9.00 K for the simulation and a maximum deficit of 12.8 K from the StickNets occurs at the verification time period. Verification of the forward flank (Fig. 3) shows that the Morrison parameterization produces a cold pool with a lower virtual potential temperature than what was observed by the StickNets. The average observed cold pool virtual potential temperature deficit in the forward (rear) flank is 5.94 K (8.80 K) while the simulation has a virtual potential temperature deficit of 6.35 K (4.85 K).

Milbrandt-Yau Parameterization

The simulation using the MY parameterization yields a supercell with a larger forward flank cold pool and lower reflectivity values than observed. The same verification time is used as in the Morrison simulation (2326 UTC) as both simulations evolved very similarly (Fig. 4).

The largest deficit of virtual potential temperature in the MY simulation is 7.07 K while the maximum deficit observed by the StickNets is 12.8 K. Again the simulation has a warmer minimum than is observed. The simulated forward (rear) flank has an average virtual potential temperature deficit of 3.29 K (-4.99 K) (Fig. 5). The simulated forward flank is warmer than the observed forward flank, however the rear flank of the simulated supercell has a colder cold pool than was observed by the StickNets.

Comparison

The verification results show that the Morrison parameterization preforms better than the MY parameterization in the forward flank, while the opposite it true for the rear flank (Table 1). Both simulations have similar evolution and have very similar vertical velocities (Fig. 6).

Due to the similar maturity and updraft strength of both parameterizations, the microphysical variables are looked at more closely especially to determine why one is performing better in one flank than the other. Microphysical species heavily tied to the cold pool development (rain and graupel/hail) are investigated.

Evolution of rain water mixing ratio with time for both simulations from 2100 UTC through 0000 UTC shows similarities initially. The Morrison parameterization then begins to produce more rain than the MY parameterization (Fig. 7). The increase of rain over time has a similar slope for both simulations, however the Morrison parameterization consistently produced more rain. The majority of this rain water mixing ratio increase occurs in the area around the updraft and in both the forward and rear flanks (Fig. 8). The higher amounts of rain water mixing ratio means that there is more evaporative potential in the Morrison parameterization simulation than in the MY simulation. The proximity to the updraft infers that some of this evaporating rain will occur in the rear flank region of the supercell enhancing the cold pool thermodynamic deficit of the rear flank in the Morrison parameterization simulation.

Melting graupel and hail are other major sources of cold pool production in supercells (Gilmore et al. 2004; James and Markowski 2010). The MY parameterization simulation produces more graupel mixing ratio than the Morrison parameterization simulation (Fig. 9). Again the evolution with time is very similar where the amount of graupel mixing ratio increases with a similar slope for both simulations. The major difference between the two simulations is the location of the graupel within the supercell. The Morrison parameterization has little graupel/hail in the rear flank, contrary to the MY parameterization, while the forward flank has more graupel/hail throughout the entirety of the forward flank (Fig. 10). Since there is less graupel/hail in the rear flank of the storm, evaporation of rain is the dominant method of rear flank cold pool production for the Morrison parameterization simulation. Also, the forward flank of the MY parameterization is larger and, because there is more graupel than rain in the forward flank, those particles are melting slower and producing a warmer cold pool than in the Morrison parameterization simulation.

4. Conclusions and future work

Two EnKF simulations, each using a different two-moment bulk microphysical parameterization, were conducted using WRF-DART and assimilating radar data. These simulations were verified against high-resolution observations from a StickNet array for a supercell that was observed on 18 May 2010. The differences between supercell cold pools developed by the two different microphysical simulations are investigated in this study.

The Morrison parameterization simulation produces a cold pool that is colder than the StickNet observations. The forward flank of the Morrison parameterization produces a result close to the observed deficit, but is still cooler than the observed deficit by 0.41 K. The larger deficit of the rear flank cold pool is attributed to the high amounts of rain water mixing ratio surrounding the updraft of the simulated supercell. This allows for more evaporatively cooled air to fall into the rear flank producing a colder-than-observed rear flank cold pool.

The MY parameterization simulation produces a warmer cold pool than is observed by the StickNet array. The rear flank of the simulated supercell is close to the observed StickNet value and is only warmer by 0.14 K. The MY parameterization produces more graupel/hail allowing for a larger forward flank. Melting of graupel/hail and subsequent evaporation of rain was slower due to the larger amount of graupel suspended above the freezing level, helping to produce a warmer forward flank.

A simulation using a single-moment microphysical parameterization will be completed to aid in the verification and justification for using a more sophisticated microphysical parameterization. Further investigation of the hydrometeor species is ongoing to fully understand why the cold pool is being produced for each simulation. In addition, another VORTEX2 event (11 June 2009) will be simulated and the supercell cold pool will be verified using the same methodology. Simulations changing fall speed, drop breakup and water shedding will be performed to investigate the impact of those values held as constants in each microphysical parameterization.

5. Acknowledgements

This study is funded by NSF grant AGS-08000542. The authors with to thank, Drs. Glen Romine, Chris Snyder, Jeffery Anderson for their assistance with the DART system. Dr. Daniel Dawson II Dr. Robin Tanamachi, Pat Skinner, and Ryan Sobash for their conversations about this work. Mike Biggerstaff and Lou Wicker for providing the mobile radar data used in this study. We would like to acknowledge high-performance computing support provided by NCAR's Computational and Information Systems Laboratory, sponsored by the National Science Foundation.

References

Biggerstaff, M. I. and Coauthors, 2005: The shared mobile atmospheric research and teaching radar: a collaboration to enhance research and teaching. *Bulletin of the American Meteorological Society*, **86**, 1263–1274, doi:10.1175/BAMS-86-9-1263.

Bryan, G. H., and H. Morrison, 2012: Sensitivity of a simulated squall line to horizontal resolution and parameterization of microphysics. *Monthly Weather Review*, **140**, 202–225, doi:10.1175/MWR-D-11-00046.1.

Dowell, D. C., and L. J. Wicker, 2009: Additive noise for storm-scale ensemble data assimilation. *Journal of Atmospheric & Oceanic Technology*, **26**, 911–927.

Gilmore, M. S., J. Straka, and E. N. Rasmussen, 2004: Precipitation and evolution sensitivity in simulated deep convective storms: comparisons between liquid-only and simple ice and liquid phase microphysics. *Monthly Weather Review*, **132**, 1897–1915.

James, R. P., and P. M. Markowski, 2010: A numerical investigation of the effects of dry air aloft on deep convection. *Monthly Weather Review*, **138**, 140–161.

Milbrandt, J. A., and M. K. Yau, 2005: A multimoment bulk microphysics parameterization. part i: analysis of the role of the spectral shape parameter. *Journal of the Atmospheric Sciences*, **62**, 3051–3064.

Milbrandt, J. A., and M. K. Yau, 2006a: A multimoment bulk microphysics parameterization. part iii: control simulation of a hailstorm. *Journal of the Atmospheric Sciences*, **63**, 3114–3136.

Milbrandt, J. A., and M. K. Yau, 2006b: A multimoment bulk microphysics parameterization. part iv: sensitivity experiments. *Journal of the Atmospheric Sciences*, **63**, 3137–3159.

Morrison, H., and J. Milbrandt, 2011: Comparison of two-moment bulk microphysics schemes in idealized supercell thunderstorm simulations. *Monthly Weather Review*, **139**, 1103–1130, doi:10.1175/2010MWR3433.1.

Morrison, H., G. Thompson, and V. Tatarskii, 2009: Impact of cloud microphysics on the development of trailing stratiform precipitation in a simulated squall line: comparison of one- and two-moment schemes. *Monthly Weather Review*, **137**, 991–1007, doi:10.1175/2008MWR2556.1.

Shabbott, C. J., and P. M. Markowski, 2006: Surface in situ observations within the outflow of forward-flank downdrafts of supercell thunderstorms. *Monthly Weather Review*, **134**, 1422–1441.

Skamarock, W. C., J. B. Klemp, J. Dudhia, D. O. Gill, D. M. Barker, W. Wang, and J. G. Powers, 2005: A description of the advanced research wrf version 2. *NCAR Technical Note*, 100.

Table 1: Virtual potential temperature deficit from the inflow for the simulations and observed used for the verification.

	Morrison	StickNet	Milbrandt-Yau
Forward flank	6.35 K	5.94 K	3.29 K
Rear flank	8.80 K	4.85 K	4.99 K
Max deficit	9.90 K	12.80 K	7.07 K

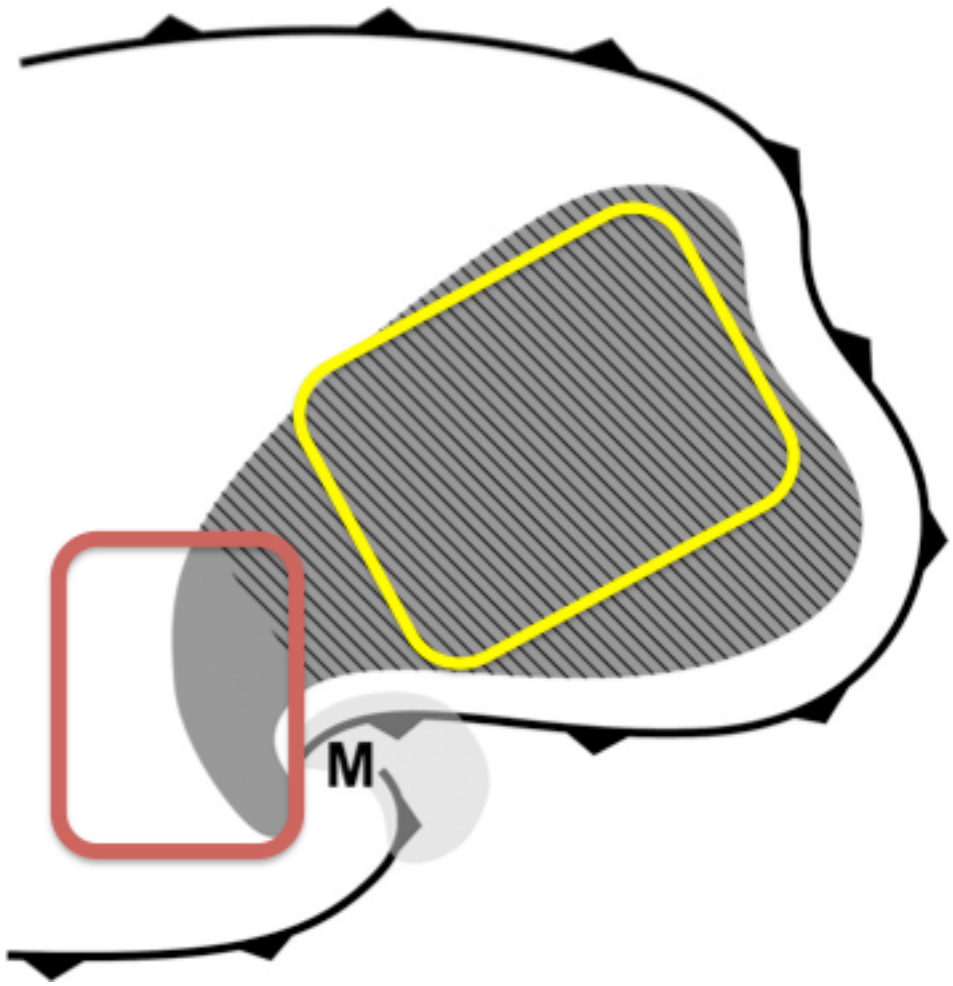

Fig. 1: Representation of the forward flank (yellow) and the rear flank (red) of an idealized supercell. Adapted from Shabbott and Markowski (2006).

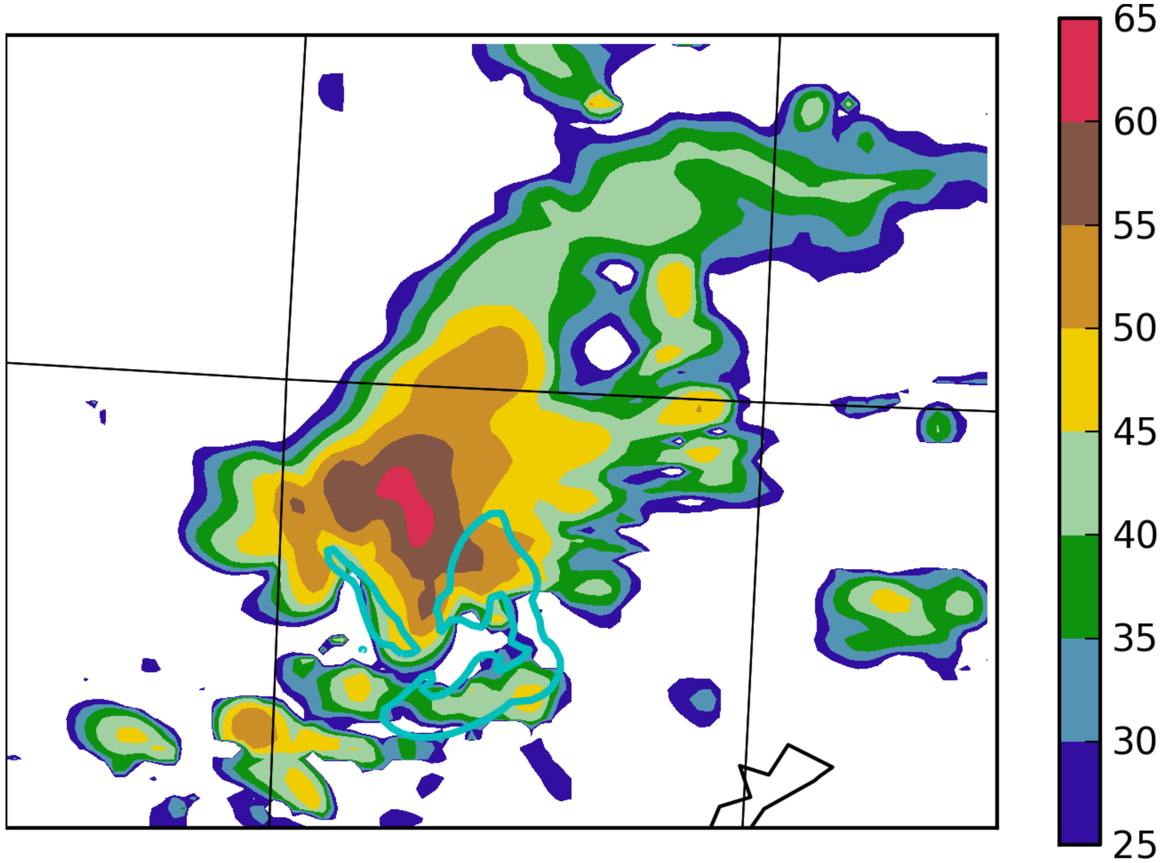

Fig. 2: Model derived reflectivity (dBZ) of the supercell at the time of verification in the Morrison microphysics simulation. Vertical velocity above 2 m s^{-1} is outlined in blue.

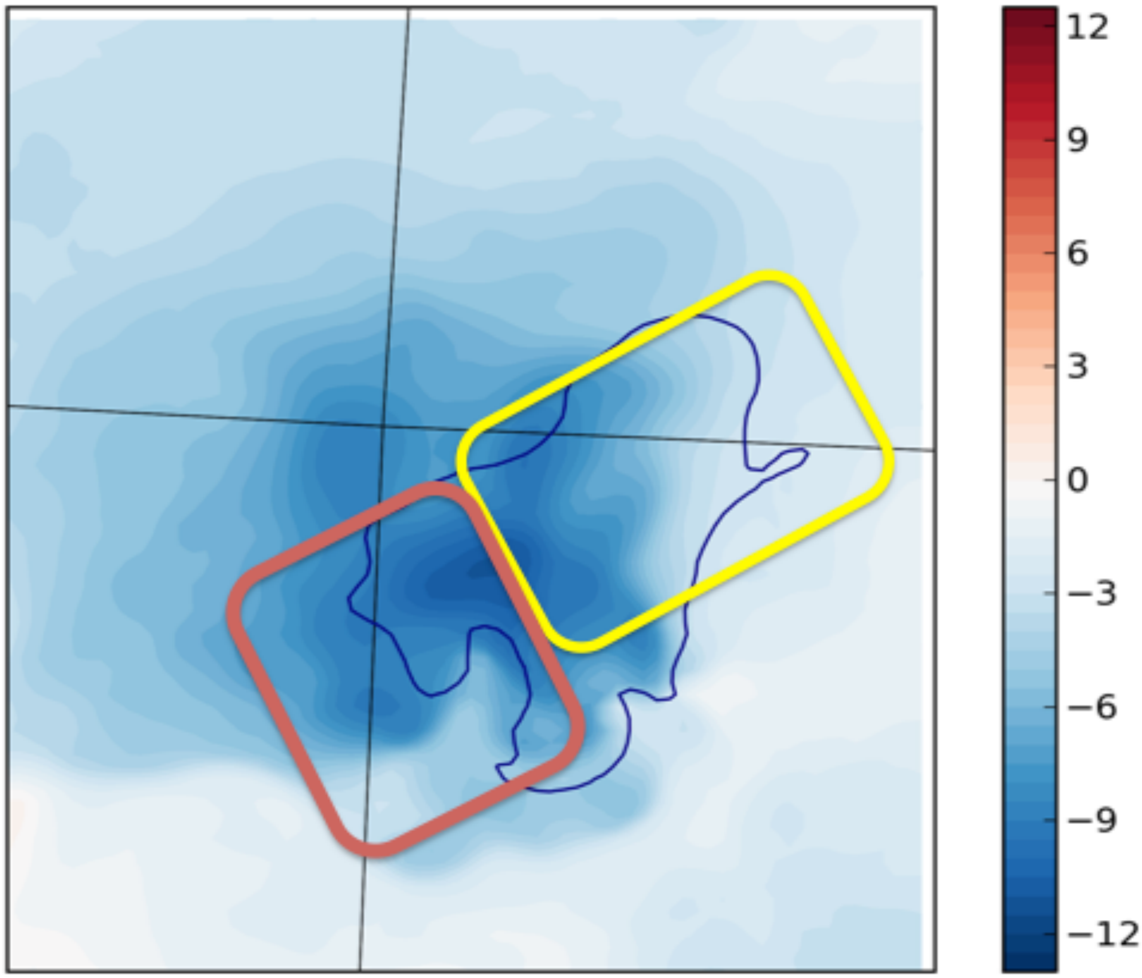

Fig. 3: Virtual potential temperature perturbation (K) from the inflow of the supercell cold pool at the time of verification from the Morrison parameterization simulation. The yellow box outlines the forward flank and the rear flank is outlined with the red box. The blue contour line is the 0.001 kg kg^{-1} Qrain contour.

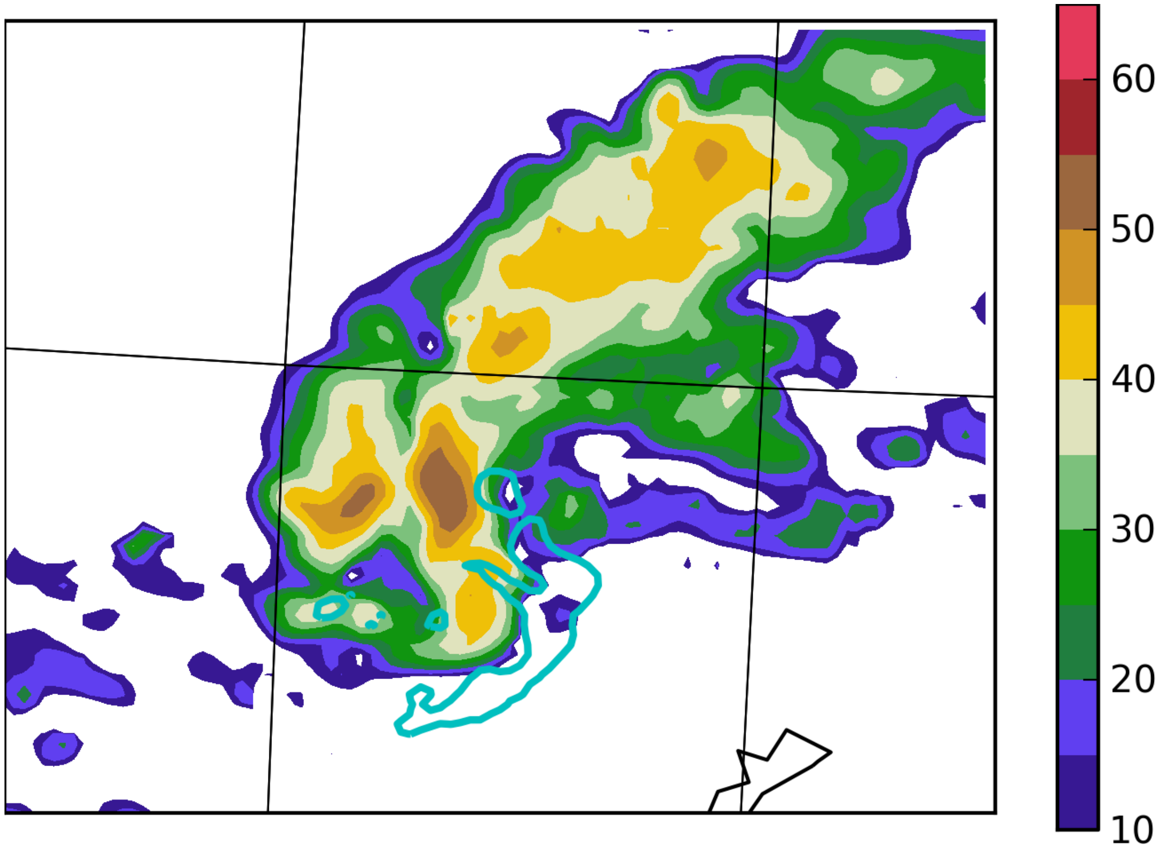

Fig. 4: Model derived reflectivity (dBZ) of the supercell at the time of verification in the MY microphysics simulation. Vertical velocity above 2 m s^{-1} is outlined in blue.

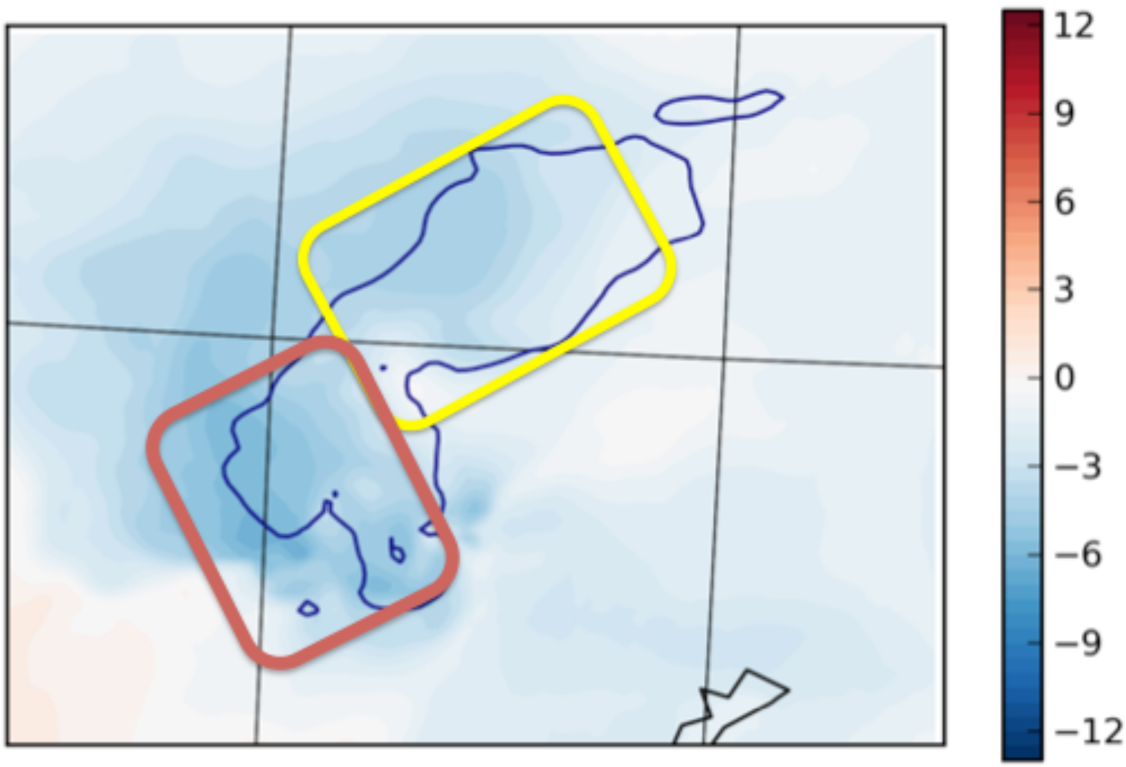

Fig. 5: Virtual potential temperature perturbation (K) from the inflow of the supercell cold pool at the time of verification from the MY parameterization simulation. The yellow box outlines the forward flank and the rear flank is outlined with the red box. The blue contour line is the 0.001 kg kg^{-1} Qrain contour.

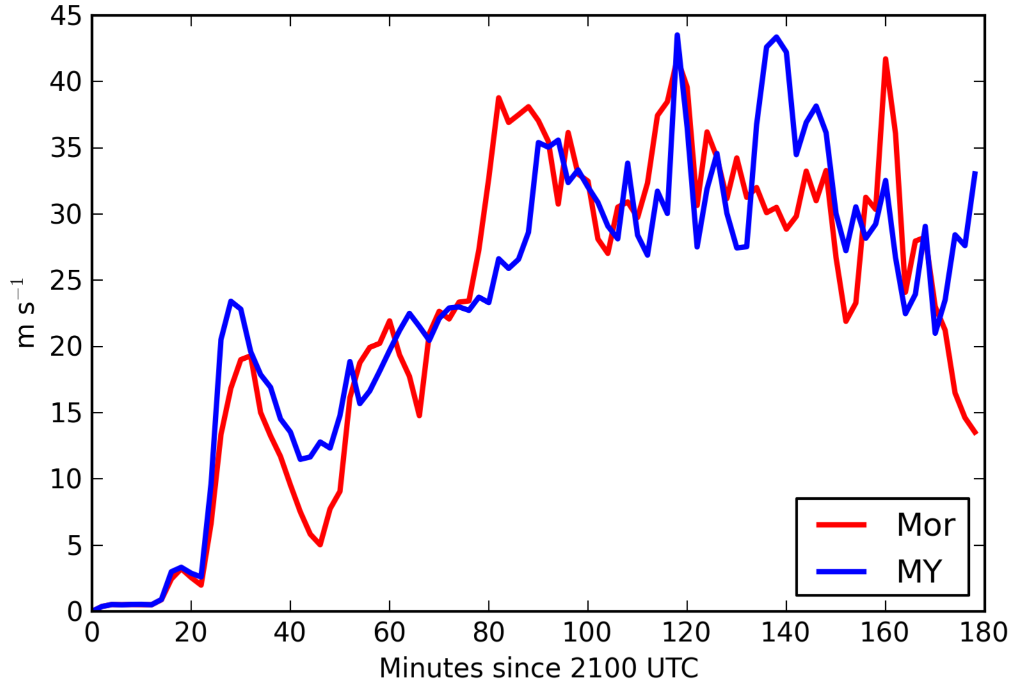

Fig. 6: Ensemble mean maximum vertical velocity (m s^{-1}, 0-8 km AGL) from 2100 UTC on 18 May 2010 through 0000 UTC 19 May 2010. The blue line represents the MY simulation, while the red line represents the Morrison simulation.

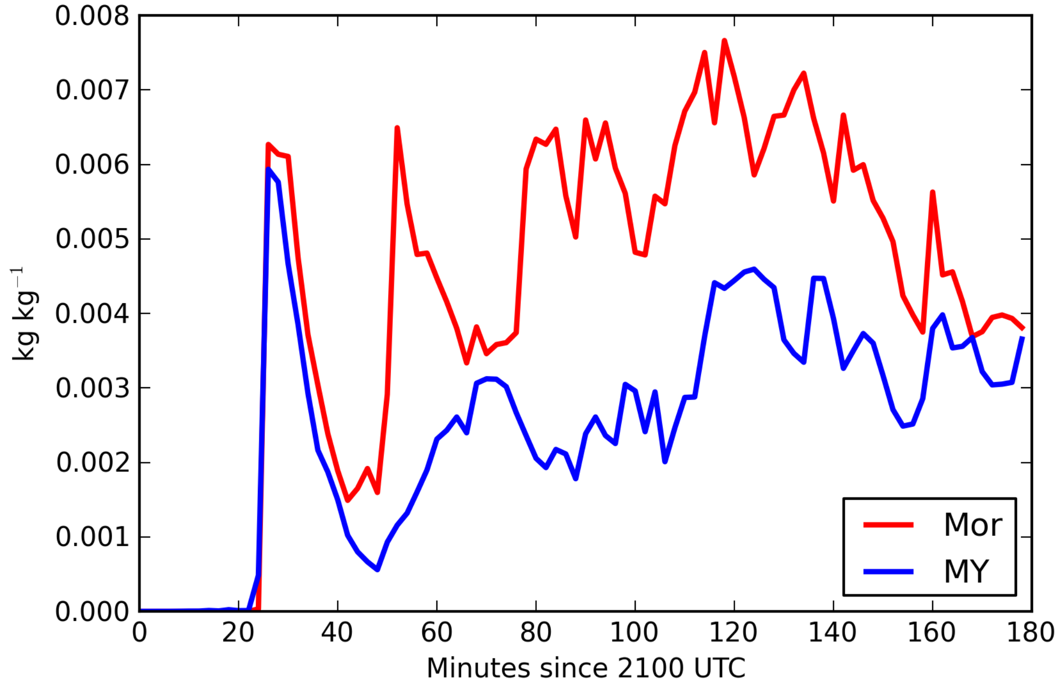

Fig. 7: As in Fig. 6, but for ensemble mean maximum Qrain (kg kg^{-1}, 0 - 12 km AGL).

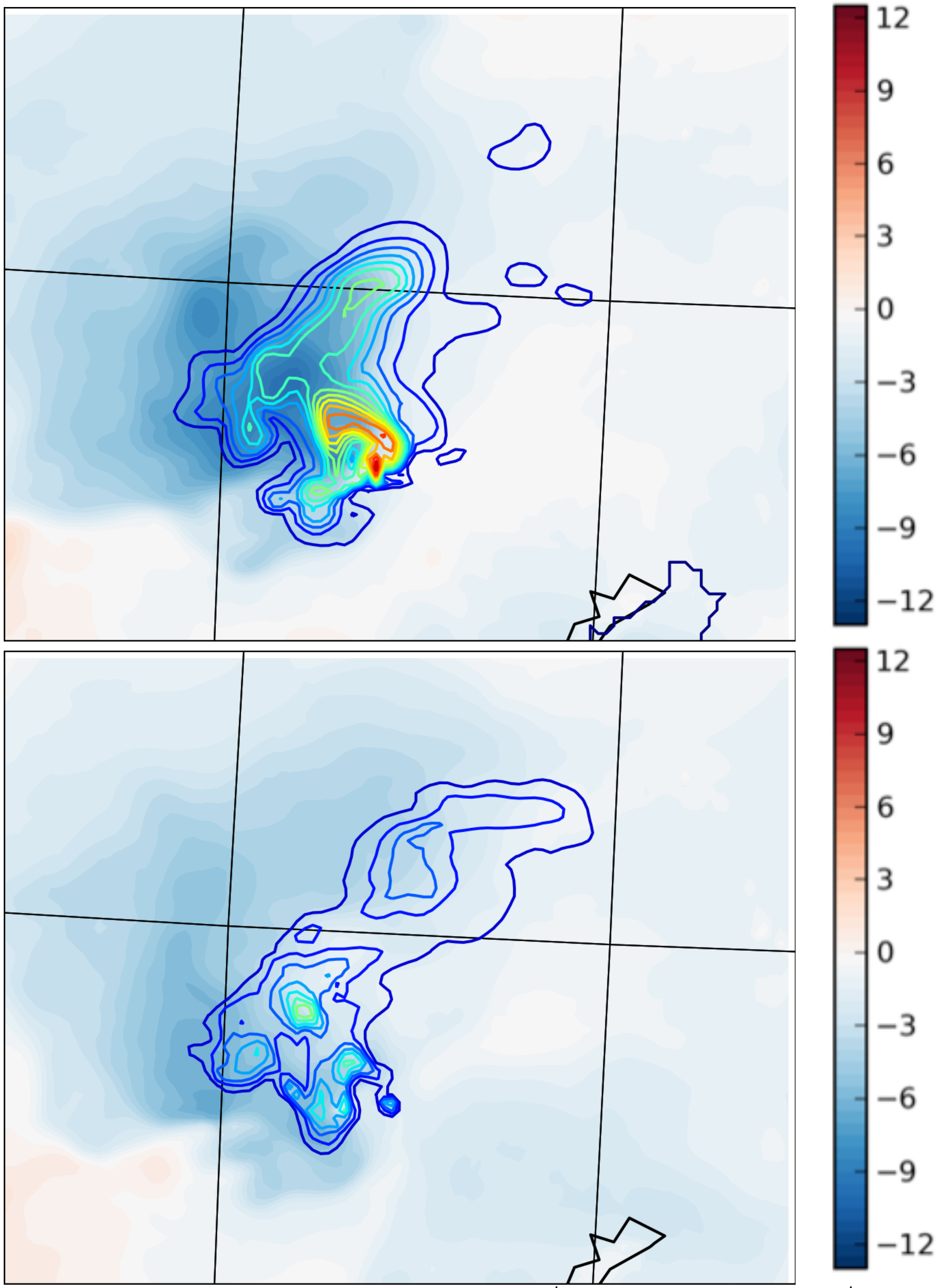

Fig. 8: Maximum ensemble mean Qrain (kg kg^{-1}) from 0 to 0.0075 kg kg^{-1} (contoured every 0.00005 kg kg^{-1}) at the time of verification for the Morrison parameterization (top) and the MY parameterization (bottom). Virtual potential temperature deficit (K) is shaded.

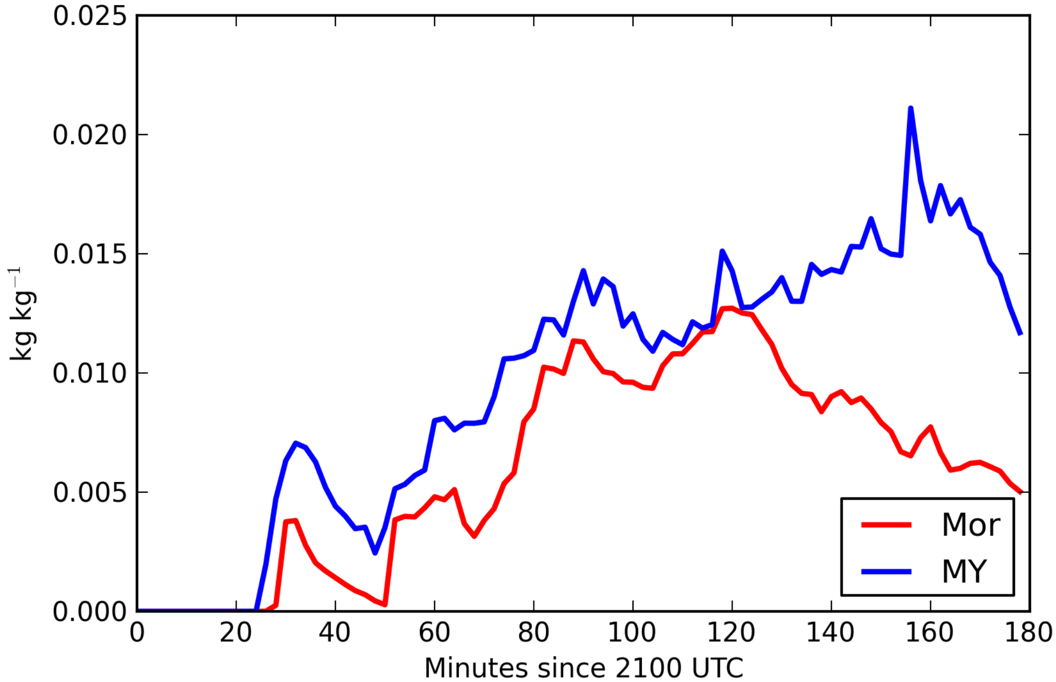

Fig. 9: As in Fig. 6, but for ensemble mean maximum Qgraupel (kg kg^{-1}, 0 - 12 km AGL).

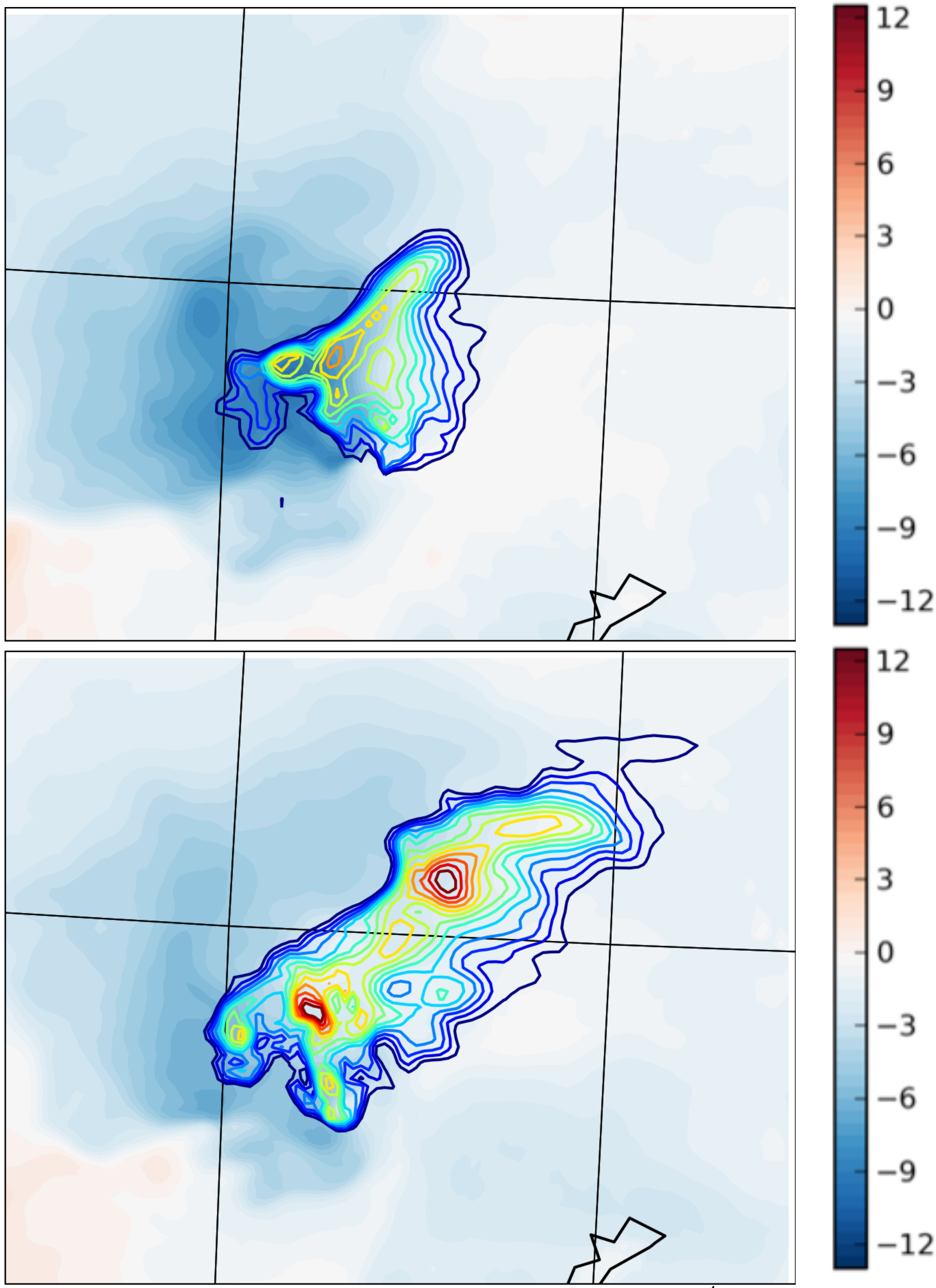

Fig. 10: As in Fig. 8, but for contour lines of Qgraupel (kg kg^{-1}).